Applied Catalysis B: Environmental 225 (2018) 538–549

Contents lists available at ScienceDirect

Applied Catalysis B: Environmental

journal homepage: www.elsevier.com/locate/apcatb

Effect of preparation method on the performance of silver-zirconia catalysts for soot oxidation in diesel engine exhaust

L. Nossova[a,*], G. Caravaggio[a], M. Couillard[b], S. Ntais[c]

[a] Natural Resources Canada (NRCan), CanmetENERGY-Ottawa, 1 Haanel Drive, Ottawa, ON, K1A 1M1 Canada
[b] National Research Council Canada (NRC), Energy, Mining and Environment Portfolio, 1200 Montreal Road, Ottawa, ON, K1A 0R6, Canada
[c] Centre for Catalysis Research and Innovation (CCRI), University of Ottawa, 161 Louis-Pasteur, Ottawa, ON, K1N 6N5 Canada

ARTICLE INFO

Keywords:
Catalyzed diesel particulate filter
Passive regeneration
Soot oxidation
Ag/ZrO_2 catalyst

ABSTRACT

This paper presents a study on the effect of the preparation method on silver-zirconia (Ag/ZrO_2) catalysts' physicochemical characteristics and their activity for soot oxidation in diesel engine exhaust. Two series of Ag/ZrO_2 catalysts with different molar fractions of Ag (5–30 mol%) were prepared by incipient wetness impregnation (IM) and citric acid-assisted sol-gel (SG) methods The catalysts were characterized using Brunauer-Emmett-Teller (BET) surface area analysis, X-ray diffraction (XRD), O_2 chemisorption, scanning electron microscopy (SEM), high resolution transmission electron microscopy (HR-TEM), X-ray photoelectron spectroscopy (XPS) and O_2 temperature-programmed desorption (O_2-TPD) techniques. The characterization results showed that silver was present mainly in the metallic state demonstrating heterogeneity in the Ag particle size distribution. XRD experiments indicated the presence of a tetragonal zirconia phase in Ag/ZrO_2-SG catalysts. Soot oxidation activity of the silver-zirconia catalysts was evaluated by temperature-programmed oxidation (TPO) in presence of 10 vol% oxygen using carbon black (CB) as model soot. Catalytic activity was shown to be dependent on the method of preparation and silver loading. The synergetic effect of metal and support on the reaction was higher for the SG catalysts. The SG catalyst containing 30 mol% Ag exhibited the best catalytic performance for CB oxidation during TPO experiments. Adsorption properties of catalysts were evaluated with the O_2-TPD. The amounts of desorbed oxygen correlated very well with the values of T_{max} obtained in TPO runs indicating that adsorbed atomic oxygen played a major role in the mechanism of CB oxidation. Testing of the best catalyst under simulated diesel exhaust conditions revealed improved CB oxidation activity in the presence of water and no detrimental effect from SO_2. These experiments showed that the new Ag/ZrO_2-SG catalyst enabled effective soot combustion under conditions that do not require NO_x. Soot removal over silver-zirconia catalysts can be an alternative method to NO-based technologies, which uses expensive Pt catalyst.

1. Introduction

A major concern with diesel vehicles is the emission of particulate matter (PM) into the atmosphere, which affects human health and contributes to climate change [1]. PM mostly consists of solid carbonaceous compounds, collectively referred to as soot, which is effectively removed from diesel exhaust by filtering with a diesel particulate filter (DPF). The critical issue of this technology is the necessity of performing active filter regeneration, a process of eliminating trapped soot particles by combustion, which is accomplished at temperatures above 600 °C. All methods used for active regeneration are normally complex and result in an increase in fuel consumption and a reduction of the DPF life. Coating the DPF with a soot oxidation catalyst lowers the temperature of soot combustion, reduces the frequency for active regeneration and allows for filter self-regeneration (passive regeneration) during normal operating conditions.

Passive filter regeneration is used in the Continuously Regenerating Trap (CRT®), a commercially available technology introduced by Johnson Matthey [2]. The CRT® device consists of a diesel oxidation catalyst (DOC) incorporating a highly active platinum oxidation catalyst followed by an uncatalyzed DPF. The CRT® performs the combustion of PM at normal exhaust temperatures of 200–500 °C with the help of NO_2 produced by the diesel oxidation catalyst (DOC), which oxidizes NO in diesel exhaust. In order for the CRT to function effectively, the technology requires a high NO_2 to PM ratio (> 20) and a low sulphur concentration of < 50 ppm in the exhaust [3]. The modified catalyzed CRT® (CCRT®) uses an additional catalyst loaded on the filter in order to increase the amount of NO_2 during soot oxidation but this leads to the

* Corresponding author.
E-mail address: lioudmila.nossova@canada.ca (L. Nossova).

https://doi.org/10.1016/j.apcatb.2017.11.070
Received 16 June 2017; Received in revised form 20 November 2017; Accepted 26 November 2017
Available online 27 November 2017

risk of NO_2 slip.

Metals commercially used for coating the DPF usually consist of platinum group metals (PGM) often in combination with cerium/zirconium oxides. Since PGM are expensive and highly sensitive to sulphur, their substitution by a cheaper active phase is desirable. Moreover, the development of more efficient combustion technologies for diesel engines in response to new fuel economy standards has created new challenges for catalyst development. Effective catalytic performance has to be achieved for soot oxidation under conditions associated with advanced, efficient engine operation which include lower exhaust temperatures and lower concentrations of NO [4].

Numerous catalyst formulations have been examined as potential materials for soot oxidation by oxygen. Among PGM-free catalysts, silver was found to be a promising metal for oxidizing soot at typical exhaust temperatures of diesel engines [5–14]. The high activity of Ag-based catalysts for soot oxidation by oxygen was linked to the so-called "active oxygen-assisted mechanism" by which metallic silver activated oxygen through a dissociative adsorption process [5–7,9,12]. Several authors have underlined that the dispersion of silver [11,12], its morphology [6,12] and its oxidation state [5,12–14] are among the factors responsible for high activity. Most authors explained the high soot oxidation activity of silver-based catalysts by the synergy with the support [5–8,10], which could contribute to formation of active oxygen species or stabilization of silver in a particular oxidation state. All of the factors mentioned above are directly related to the preparation procedures used for catalyst synthesis.

Among the many authors that have studied supported silver catalysts for soot oxidation, most have used impregnation [5,7,9–11,14], citrate sol-gel [8,13] and co-precipitation [6] techniques for preparing these catalysts. The citrate complexation technique, a variation of the Pechini method [15], has been widely used for catalyst preparation. The complexation of catalyst precursors with citric acid provides homogeneous component mixing which is maintained during the gelation step. The subsequent thermal decomposition of a citrate gel polymer yields more effective catalysts due to a higher degree of component homogeneity than when prepared by conventional methods [16]. Guilhaume et al. [8] used the citrate method for the preparation of an $AgMnO_x$ catalyst and suggested that it provided the incorporation of silver in a mixed Ag-Mn oxide structure. As a result, a highly active and thermally stable catalyst for soot oxidation was obtained.

We expect that by using citrate complexation we will obtain silver-zirconia catalysts with improved activity due to chemical interaction of all components during preparation. The combination of Ag with zirconium oxide seems to be a promising choice to achieve the desired properties, such as high activity, due to silver and high thermal stability because of the zirconia's resistance to sintering.

The aim of the following study was to compare the physicochemical and catalytic soot oxidation properties of Ag/ZrO_2 catalysts prepared by two different methods. Two series of zirconia-supported silver catalysts with different silver contents (5–30 mol%) were prepared either by citrate sol-gel method or by incipient wetness impregnation. Catalysts were thoroughly characterized by various techniques such as BET, XRD, O_2 chemisorption, HR-TEM, SEM, XPS and O_2-TPD. The influence of the preparation method on catalyst characteristics is considered in the section on Results and Discussion. The catalyst performance for soot oxidation was conducted by temperature-programmed oxidation (TPO) using carbon black (CB) as a model of soot. The best performing catalyst was then tested in a fixed-bed reactor under simulated diesel exhaust conditions. The difference in activity between IM and SG catalysts was linked to differences in the catalyst structure and oxygen adsorption.

2. Experimental

2.1. Catalyst preparation

Ag/ZrO_2-IM catalysts were prepared by incipient wetness impregnation of commercial ZrO_2 (Sigma Aldrich) with an aqueous solution of $AgNO_3$ (Sigma Aldrich), followed by drying at 120 °C overnight and calcination at 550 °C for 6 h.

Ag/ZrO_2-SG catalysts were prepared by the citrate sol-gel method using $AgNO_3$ and $ZrO(NO_3)_2{\cdot}xH_2O$ (Sigma Aldrich) as precursors. Aqueous solutions of metal precursors were mixed together and then an aqueous solution of citric acid was added under vigorous stirring. The molar ratio of metal ions to citric acid was 1:3. The final mixture was heated to 80–90 °C under stirring to evaporate the excess water until a viscous gel was formed. Then the gel was charred at 200 °C for 12 h resulting in a brown coloured and foam-like fragile material. This product was ground with a mortar and pestle followed by calcination at 550 °C for 6 h.

The silver-zirconia catalysts were denoted as $Ag(x)/ZrO_2$, where x is the mole fraction of Ag in% (*i.e.* x = 5, 10, 20, 30) and corresponding zirconium concentrations of 95, 90, 80 and 70 mol%, respectively.

2.2. Catalyst characterization

The textural properties of silver-zirconia catalysts, such as pore size, pore volume and specific surface area, were measured by the BET N_2 adsorption method using an ASAP2010 instrument (Micromeritics Inc.). The samples were degassed at 250 °C for 5 h and N_2 adsorption was carried out at 77 K. The pore size and pore volume were calculated using the adsorption branch of the N_2 adsorption isotherm by the BJH method.

Crystal structures of resulting phases of Ag/ZrO_2 were determined by powder X-ray diffraction. Diffractograms were recorded on a Rigaku Ultima IV XRD spectrometer using Cu Kα radiation (1.54 Å) and equipped with a diffracted-beam monochromator and a high-speed semiconductor one-dimensional X-ray detector (D/teX Ultra). XRD patterns were collected over the 2θ angular range of 20–80° at a scanning rate of 1°/min and 0.01° intervals. Diffraction peaks of crystalline phases were identified using the International Center for Diffraction Data (ICDD) database. The average crystallite size was calculated based on the Scherrer equation using the Rigaku PDXL Diffraction software's whole pattern profile fitting program (WPPF).

The Ag particle size and surface area of Ag were determined by irreversible O_2 chemisorption using static volumetric method provided by a Micromeritics ASAP 2020C instrument. Prior to adsorption experiments, catalysts were first oxidized *in-situ* in O_2 flow at 170 °C and then reduced in H_2 flow at 170 °C. Analysis conditions included O_2 pressure ranges from 40 to 130 Torr, analysis temperature of 170 °C and adsorption stoichiometry of Ag/O_2 = 2 [17].

The catalyst microstructure was analyzed using a FEI Titan cubed 80–300 microscope operated at 300 kV and equipped with a CEOS aberration corrector for the probe forming lens, a monochromated field-emission gun and an EDAX energy dispersive X-ray (EDX) spectrometer for elemental analysis of selected areas. Prior to TEM examination, the samples were suspended in ethanol and sonicated for five minutes. A drop of ethanol suspension was deposited on a copper grid covered by a lacey carbon film. Ag average particle size and particle size distribution were measured using ~100 Ag particles from randomly chosen areas from the TEM images.

The samples were all imaged with a Hitachi S–3400 N scanning electron microscope (SEM) using the Oxford Instrument Aztec 2.1a software. The images were obtained at an accelerating voltage of 20 kV with a working distance of approximately 10 mm. The probe current was approximately 50 μA. All images were taken with the secondary electron detector.

XPS analysis was performed using monochromatized Al Kα (hv = 1486.6 eV). The pressure in the analysis chamber was lower than 10^{-9} mbar. The measurements were carried out using an electron gun to decrease charging effects. The C1 s XPS core level peak at 285 eV was used to calibrate the energy scale. The analysis of the O1 s and Zr3d and Ag3d XPS core level was performed using Casa XPS and XPS peak

software.

A Micromeritics AutoChem II 2920 Chemisorption Analyzer equipped with a thermal conductivity detector (TCD) was used for O_2-TPD. First, the catalyst was pretreated in 10 vol% H_2/Ar at 200 °C, then oxygen preadsorption was performed at 600 °C for 30 min in oxygen flow. After cooling down to room temperature in the same flow, the sample was flushed with He for 30 min to remove the gas phase oxygen and physically adsorbed oxygen on the Ag surface of the catalyst. The O_2-TPD profile was obtained when the catalyst was heated to 600 °C at a heating rate of 20 °C/min in a 20 mL/min He flow while monitoring the reactor effluent. Deconvolution of the TPD profiles was performed with a Gaussian model fit using the method of least squares.

2.3. Activity tests

2.3.1. Temperature-programmed oxidation (TPO)

The activity of catalysts was evaluated by TPO using a Micromeritics AutoChem II 2920 Chemisorption Analyzer. Carbon Black (CB, Monarch 120 from Cabot) was used as model soot. The samples were prepared by mixing catalyst and CB (catalyst:CB weight ratio of 30:1) together using a mortar and pestle to achieve tight contact. A 30-mg test sample of the catalyst/carbon mixture was loaded in a U-shaped quartz reactor and pretreated by heating in He flow up to 400 °C to remove impurities and water. Then, the TPO run was performed with 10 vol% O_2 in He flow at a rate of 60 mL/min in the temperature range of 35 °C to 600 °C at a heating rate of 10 °C/min. The carbon combustion products were detected by a thermal conductivity detector (TCD) throughout the entire TPO run. The catalytic activity was assessed by using a T_{max} value, the temperature at the maximum carbon oxidation rate indicated by a peak in the TPO profiles. A lower value of T_{max} corresponds to greater catalytic activity.

In order to measure the rate of the CB oxidation reaction, the same mixtures were tested under isothermal conditions at a temperature of 350 °C using a thermogravimetric analyzer (TGA TherMax 700). The initial rates of CB oxidation were calculated from the slope of a tangent line taken from the curve of carbon weight versus time for conversion values less than 5%.

2.3.2. Simulated diesel exhaust gas tests

The catalytic performance of the selected catalysts for carbon oxidation was evaluated in a fixed-bed reactor under simulated diesel exhaust gas conditions. Selected concentrations of NO, O_2 and H_2O in a flow of nitrogen as shown in Table 1 simulate diesel exhaust from heavy-duty truck engines. Chemical poisoning by sulfur was assessed by adding 10 ppm SO_2 to the full simulated exhaust.

Before testing, all catalyst-CB mixtures were pelletized and sieved to a particle size in the range of 125–180 μm (80–120 mesh sizes). The test sample of 500 mg (± 10 mg) was mixed first with 250 mg of cordierite particles of the same size in order to mitigate hot spots within the catalyst bed, and then loaded in a 6 mm quartz reactor tube between two pieces of quartz wool. The pre-treating conditions were the same as those used for the TPO runs, namely, heating the sample in helium gas at 400 °C to remove impurities. The reaction gas was supplied at a flow rate of 500 mL/min (~60 000 h^{-1} gas hourly space velocity) while the temperature was ramped from 75 °C to 600 °C at a rate of 3 °C/min. The effluent gas was analyzed using a MKS Multi Gas 2013 FTIR analyzer.

Table 1
Testing parameters and simulated diesel exhaust gas composition.

Gas component	O_2	H_2O	NO	SO_2	N_2
Concentration in N_2	10 vol%	5 vol%	500 ppm	10 ppm	Balance
Reactor temperature	75–600 °C				
Temperature ramp	3 °C/min				
Reactor GHSV	50,000–60,000 h^{-1}				

Concentrations of all gas components were plotted against temperature. The experimental error on T_{max} in concentration-temperature profiles was ± 2 °C.

Additionally, some catalysts were tested under simulated diesel exhaust conditions after soot loading from a soot generator (miniCAST Model 5201 A, Jing Ltd., Switzerland). The exhaust containing soot from the soot generator was pulled through a catalyst layer that was spread evenly on a Teflon filter.

3. Results and discussion

3.1. Texture characterization

Typical experimental adsorption-desorption isotherms of N_2 on Ag (30)/ZrO_2-IM and Ag(30)/ZrO_2-SG catalysts are shown in Supplementary Figs. S1A and S1B, respectively. According to IUPAC classification [18], both isotherms could be classified as Type IV, characteristic of a mesoporous material. The hysteresis loops presented by both isotherms were narrow with two almost vertical and parallel branches that could be assigned to H1 type. Usually, Type H1 hysteresis represents porous materials that consist of agglomerates or spherical particles which are arranged in a fairly uniform fashion with narrow distribution of pore size [18].

The surface area of each synthesized catalyst was less than 30 m^2/g (Table 2). A decrease in surface area with increasing Ag loading for SG catalysts was observed, whereas no significant changes were found for the IM catalysts. Overall, SG catalysts exhibited slightly higher surface areas compared to IM catalysts with the same composition. The pore size distribution for Ag(30)/ZrO_2-IM and Ag(30)/ZrO_2-SG catalysts is shown in the inset of Supplementary Figs. S1A and S1B, respectively. The IM sample demonstrated a narrow and monomodal distribution curve whereas the SG catalyst showed a broader monomodal distribution curve. These results correspond to mesoporous structures with the average pore diameter of 23.1 and 24.6 nm and pore volume of 0.11 and 0.13 cm^3/g for the IM and SG catalysts, respectively, as shown in Table 2. It is interesting to note that when the Ag loading increased from 5 mol% to 30 mol%, the pore size of the IM catalysts decreased from 30.5 to 23.1 nm whereas the SG catalysts demonstrated the opposite tendency with increasing pore size from 14.2 to 24.6 nm. Moreover, the pore volume of IM catalysts decreased with increase in Ag loading. However, the variation in average pore volume of the SG catalysts did not show any trend depending on Ag loading. It is evident that for the IM catalyst, the Ag precursor enters the pores of the support thus reducing the overall pore size and volume. In the case of SG catalysts, the final structure of the material is controlled by a different formation mechanism during the citrate sol-gel preparation, independent of Ag loading in the concentration range used in this study.

3.2. Structure analysis by XRD

The structure of the phases for the Ag-ZrO_2 catalysts was identified by XRD analysis. After calcination at 550 °C, all the samples exhibited characteristic peaks at 38.1° and 44.3° that were assigned to diffraction lines of the (111) and (200) planes of metallic Ag, a face-centered cubic crystal structure (Fig. 1). The average crystal lattice parameter of Ag (111) was 4.08 Å which matched the Ag powder lattice parameter in the ICDD database (PDF 03-0635-2871). The remaining peaks in the XRD patterns of the IM catalysts were assigned to a monoclinic crystal structure of zirconia (m-ZrO_2) characterized by the intensive diffraction peaks at $2\theta = 28.2°$ and $2\theta = 31.5°$ (PDF 01-083-0943). The XRD patterns for the SG catalysts indicated a mixture of two zirconia phases. The minor zirconia phase was the monoclinic zirconia structure. The major zirconia phase was assigned to the tetragonal structure (t-ZrO_2) with a characteristic peak at about $2\theta = 30.2°$ (PDF 01-070-8758). It should be mentioned that the position of the XRD diffraction peaks for tetragonal and cubic structures of zirconia are very similar. However,

Table 2
Textural properties of Ag/ZrO_2 catalysts and Ag particle size.

Sample	S_{BET} (m^2/g)	V_p[a](cm^3/g)	D_p[b](nm)	Ag particle size		Ag Surface Area[e] (m^2/g Ag)
				d_{XRD}[c](nm)	d_{CHEM}[d](nm)	
ZrO_2 commercial	23.4	0.17	25.4	n.a.[f]	n.a.	n.a.
$Ag(5)/ZrO_2$-IM	17.9	0.18	30.5	62.6	11.7	49.0
$Ag(10)/ZrO_2$-IM	17.0	0.17	30.2	67.2	19.9	28.7
$Ag(20)/ZrO_2$-IM	18.0	0.12	23.5	63.1	44.4	12.9
$Ag(30)/ZrO_2$-IM	16.8	0.11	23.1	70.4	78.8	7.3
$Ag(5)/ZrO_2$-SG	25.1	0.12	14.2	34.2	8.4	68.1
$Ag(10)/ZrO_2$-SG	25.7	0.13	16.8	42.1	15.9	35.9
$Ag(20)/ZrO_2$-SG	21.4	0.15	23.1	68.4	27.5	20.8
$Ag(30)/ZrO_2$-SG	18.2	0.13	24.6	78.8	44.8	12.7

[a] BJH desorption cumulative pore volume.
[b] BJH desorption average pore diameter.
[c] Calculated from XRD data using the Scherrer equation.
[d] Calculated based on stoichiometry factor of $Ag/O_2 = 2$.
[e] Calculated from O_2-chenisorption data.
[f] not applicable.

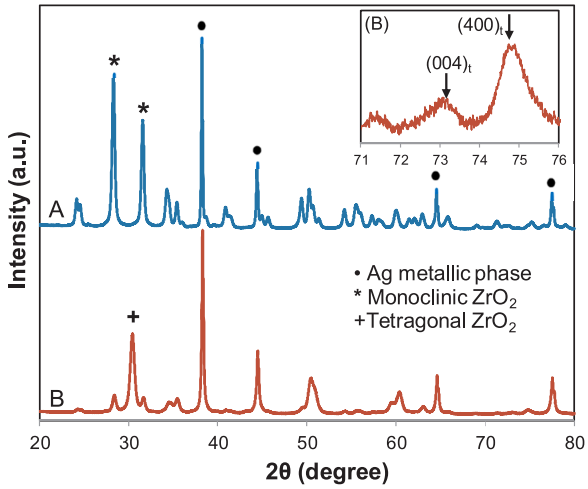

Fig. 1. XRD patterns of $Ag(30)/ZrO_2$-IM (A) and $Ag(30)/ZrO_2$-SG (B) catalysts.

the formation of t-ZrO_2 phase in the SG samples was supported by the presence of the characteristic splitting of the (400) line in the 2θ region from 71 to 76° into (400) and (004) lines (shown in Fig. 1 inset) [19]. Additionally, the formation of the cubic form of zirconia was less probable because of its weak stability in the temperature ranges used in this study [20].

The phase content in the SG catalysts was estimated from the XRD patterns using the Rietveld method. A ZrO_2 sample synthesized by the SG method was also analyzed for comparison. The results are shown in Table 3 along with the crystal sizes of the zirconia phases and lattice parameters for the t-ZrO_2 phase. As can be seen from the table, the bare ZrO_2.SG contains 48 wt% of the t-ZrO_2 phase. With the addition of Ag, the content of the t-ZrO_2 increased significantly to approximately 80 wt %. The higher Ag content in the SG catalysts accompanied a decrease in lattice dimensions compared to the ZrO_2-SG that could be associated to the formation of oxygen vacancies according to Grabowski et al. [21]. Those authors explained the stabilization of t-ZrO_2 phase in the catalysts by the presence of these vacancies. The results reported in this work are in agreement with modelling calculations confirming the presence of oxygen vacancies which stabilize tetragonal and cubic forms of ZrO_2 [22].

Another proposed mechanism to stabilize undoped t-ZrO_2 is to control the crystallite size of the tetragonal phase to be smaller than < 30 nm [23]. As shown in Table 3, for all the SG catalysts, an average crystallite size of t-ZrO_2 phase was found to be in the range of

Table 3
Results of Rietveld XRD analysis for the Ag/ZrO_2-SG catalysts (t- tetragonal, m- monoclinic).

Catalyst	t-ZrO_2 phase (wt%)	Lattice parameters of t-ZrO_2 (a x a x c)		Crystallite size[a] (nm)	
		a (Å)	c (Å)	t-ZrO_2	m-ZrO_2
ZrO_2-SG	48	3.600	5.189	8.6	13.1
$Ag(5)/ZrO_2$-SG	78	3.602	5.187	10.0	12.6
$Ag(10)/ZrO_2$-SG	77	3.599	5.187	10.3	12.6
$Ag(20)/ZrO_2$-SG	89	3.593	5.171	7.3	8.3
$Ag(30)/ZrO_2$-SG	83	3.579	5.130	7.5	9.6
ZrO_2 comm.	0	n.a.[b]	n.a.	n.a.	20.9

[a] Calculated by the Scherrer equation.
[b] not applicable.

7.3–10.3 nm. The corresponding average crystallite size of the monoclonal zirconia in the SG samples was found to be slightly larger than in t-ZrO_2. By comparison, the m-ZrO_2 phase in the IM catalysts showed an average crystallite size of approximately 20 nm (see commercial ZrO_2 in Table 3). The effect of crystallite size on phase formation in pure zirconia was thoroughly reviewed by Kurapova et al. [24]. The authors showed that the synthesis method significantly influenced the critical crystallite size as well as the phase crystallization temperature and the final zirconia composition.

Silver particle sizes were estimated using the Scherrer equation and summarized in Table 2. There were negligible differences in Ag particle sizes for the IM catalysts with varying Ag loading. In contrast, for the SG catalysts, an increase in the Ag particle size from 34.2 nm to 78.8 nm was detected as the Ag concentration increased from 5 to 30 mol%. These discrepancies in XRD data between IM and SG catalysts can be explained by the limitations of the XRD method. If the sample had a non-uniform particle size distribution, the sharp peak of the larger particles determined the width of the diffraction peaks that were used for the particle size calculations. Thus, based on the XRD Ag size values, we could not unequivocally draw a conclusion regarding the effect of the preparation method on the Ag particle size. Overall, the calculated average Ag particle sizes for both IM and SG catalysts were less than 80 nm (Table 2).

To summarize the XRD results, it is concluded that the tetragonal zirconia produced during the citrate sol-gel preparation method was stabilized by a small zirconia crystallite size and the formation of

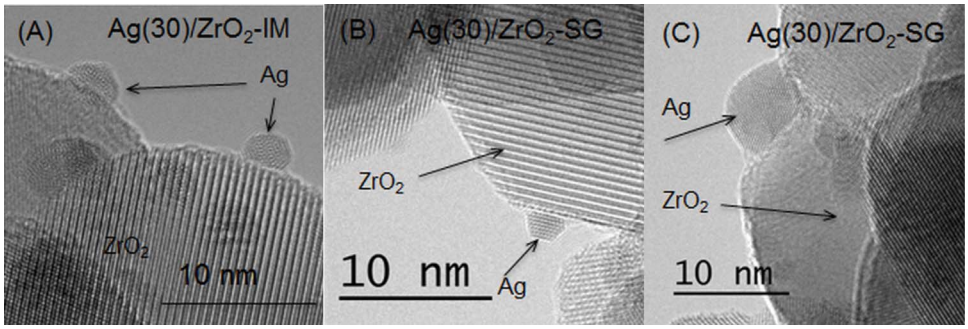

Fig. 2. TEM images of silver particles in the Ag(30)/ZrO_2 catalysts showing a twining defects (A), a single domain of metallic silver (B) and a silver multigrain particle (C) marked by arrows.

oxygen vacancies.

3.3. Ag particle size by TEM, SEM and O_2 chemisorption

The Ag-ZrO_2 catalysts were characterized by high-resolution TEM (HR-TEM) analysis in order to investigate the morphology and particle size distribution of Ag. Fig. S2 presents the comparison of TEM images between IM and SG catalysts of the lowest 5 mol% and highest 30 mol% Ag loading. TEM micrographs (Fig. S2) clearly showed the presence of Ag nanoparticles of ~2–5 nm in diameter regardless of the preparation method and Ag content.

Detailed analysis of the HR-TEM micrographs of the Ag(30)/ZrO_2-IM and Ag(30)/ZrO_2-SG catalysts identified that both catalysts had small Ag particles of ~2–4 nm in diameter (Fig. 2A and B). The observed hemispherical shape indicated the tendency towards Ag particles "wetting" the substrate surface, in other words, contact between the silver particles and their support occurred. The latter might be important if both the metallic particle and support contribute to catalysis. The TEM images also illustrated monocrystalline or polycrystalline structures with twining defects (Fig. 2A and B). As shown in Fig. 2C, the particle of ~8 nm in the SG catalyst possessed a polycrystalline structure with a number of grain boundaries and other structural defects. Thus, it appears that the preparation method influenced the size, number and morphology of Ag particles especially at higher concentration of Ag when the formation of larger particles was more probable.

The Ag particles were also characterized using an annular dark-field (ADF) scanning TEM (STEM). The images acquired at a lower magnification clearly showed the presence of a few larger Ag particles in both SG and IM catalysts. The large Ag particles were in the range from 20 to 100 nm (Fig. S3). Specific EDXS scans were made for large particles detected in ADF STEM images. Metallic Ag was found to be the predominant species in the particle 1A of the IM catalyst and the particle 1B of the SG catalysts in Fig. S3 whereas particles 2A and 2B consisted of mostly zirconia. Thus, the TEM data showed that both IM and SG catalysts were very heterogeneous in terms of the Ag particle size distribution, which included small and very big particles.

Complementary to the TEM studies of smaller particles, SEM imaging analysis of larger particles were undertaken. SEM mapping images of the Ag(30)/ZrO_2-IM and Ag(30)/ZrO_2-SG catalysts are shown in Fig. 3. Large Ag particles in the IM catalyst were found to have irregular shapes and sizes in the range of 3–5 μm. The SG catalyst consisted of numerous spherical silver particles with small diameters of < 0.5 μm and a small amount of larger particles of 2–3 μm that were both smaller than those of the IM catalyst.

The TEM and SEM analyses did not allow a conclusion about the average Ag particle size in the catalysts due to the non-uniform particle size distribution and the local nature of both methods. Therefore, the Ag particle size was also measured by O_2-chemisorption which produced average values among the nanometer- and micrometer-size particles. As shown in Table 2, the average size of Ag increased with Ag loading for both IM and SG catalysts. However, SG catalysts demonstrated lower Ag particle sizes compared to IM catalysts with the same composition.

Finally, results shown in this section suggest that these two preparation methods led to different morphologies, number, and sizes of Ag particles in the catalysts of the same Ag content. Consequently, it is expected that these catalysts may perform differently in oxygen activation and as a result in soot oxidation.

3.4. Surface analysis by XPS

XPS measurements were carried out to define the chemical state of the elements in the near-surface region of the Ag(30)/ZrO_2-IM and Ag(30)/ZrO_2-SG catalysts (Figs. 4 and 5, Table 4). Fig. 4 shows the XPS spectra of O 1s, C 1s and Zr 3d core levels for both catalysts. The analysis of the O 1 s peak revealed the existence of three components with the corresponding binding energy (BE) values of 530.1 (O^I), 531.9 (O^{II}) and 533.2 eV (O^{III}). The position of O^I is characteristic of lattice oxygen atoms in ZrO_2 [21,25,26] but it might contain a small contribution from atomic oxygen chemisorbed on the silver surface [27,28]. The O^{II} component is related to oxygen in hydroxyls (–OH) at the surface and C—O species as reported in similar studies [21,26], while it has been assigned to physically adsorbed oxygen [29]. The O^{III} component is attributed to $-CO_3$ and/or adsorbed water. The three components had relative intensities of $O^I/O^{II}/O^{III}$ = 62/25/13 for the catalysts prepared using the IM method while they slightly changed to 66/25/9 for the SG sample (Table 4).

Analysis of C 1s XPS peaks revealed the existence of three components (Fig. 4) with BE values of 285, 286.5 and 289 eV in both IM and SG samples due to C—C, C═O and free COO— species, respectively [21]. The positions of C 1s peaks and their relative intensities did not change significantly when IM and SG samples were compared. Therefore, the preparation method appeared to have no influence on the presence of carbon on the catalyst surface and C 1s peaks were related to the adsorption of hydrocarbons and CO_2 from the ambient environment.

Analysis of the Zr 3d peak was performed using doublets with spin orbit splitting of 2.4 and an intensity ratio of Zr $3d_{5/2}$: Zr $3d_{3/2}$ = 3:2 [30]. The Zr $3d_{5/2}$ XPS peak fitting of the IM and SG catalysts resulted in two components (Zr^I and Zr^{II}) representing two types of zirconium species in the catalysts. The Zr^I component of the IM catalyst with lower BE of 182.1 eV comprised 90% of the overall Zr $3d_{5/2}$ intensity and was attributed to Zr^{4+} in ZrO_2. The SG sample comprised 88% of ZrO_2 in accordance with the Zr^I peak position and intensity. According to the literature, the less intense Zr^{II} component with higher BE of 183.2 eV can be assigned to Zr atoms in zirconium surface carbonates Zr—O—C or to partially reduced $Zr^{\delta+}$ sites [31,32]. No difference in Zr^{II} confirmed that the signal of Zr^{II} component was not related to the preparation procedure but rather to atmospheric contamination. The calculated O:Zr atomic ratios (Table 4) was 2.5 and 2.3 for the IM and SG catalysts, respectively. The lower O:Zr ratio for the SG catalyst supports the assumption that higher surface concentration of oxygen vacancies were in this sample. Further studies would be necessary to gain a better insight

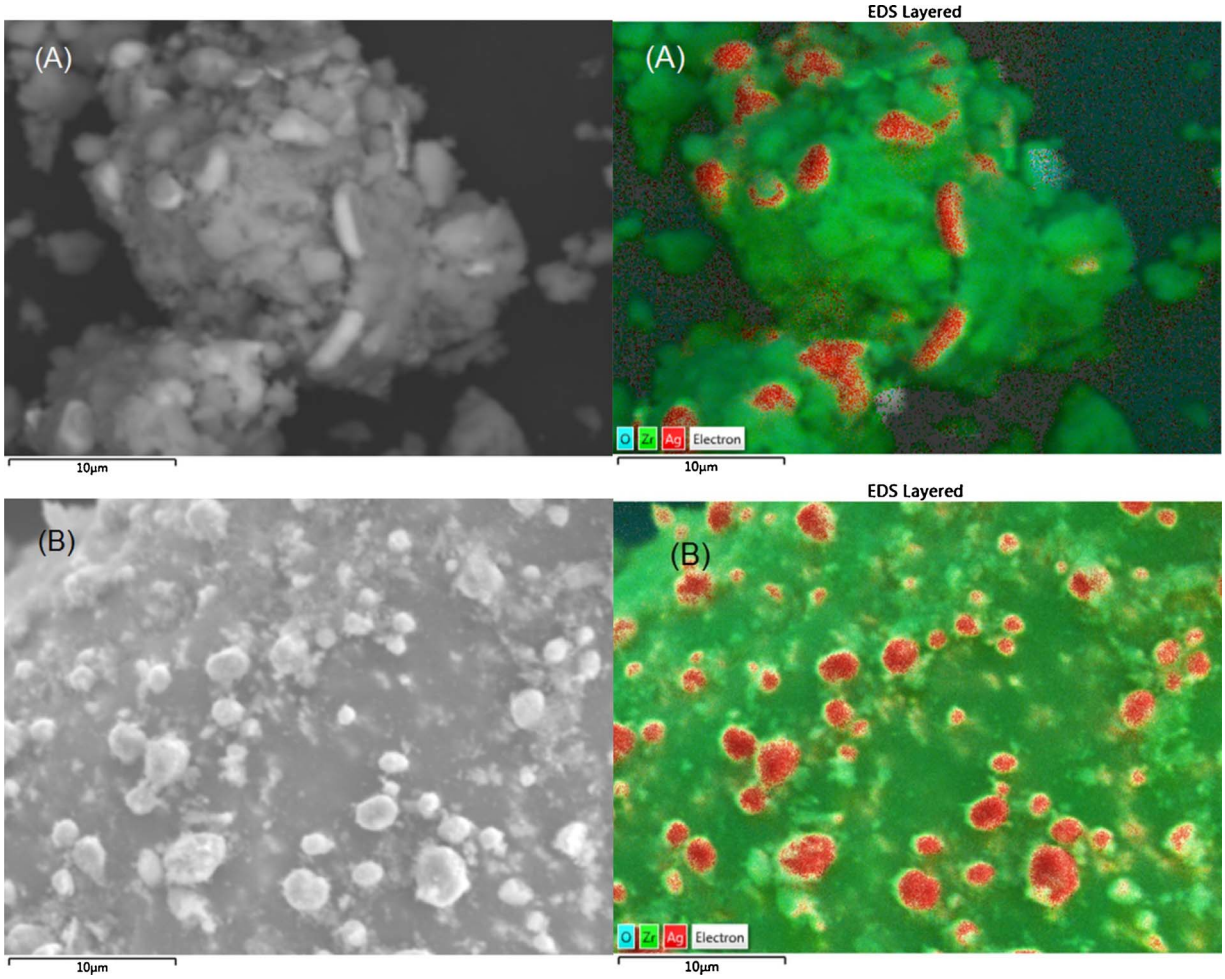

Fig. 3. SEM images of silver particles in the Ag(30)/ZrO_2-IM (A) and Ag(30)/ZrO_2-SG (B) catalysts and corresponding EDS layered data.

into the relationship between XPS data and oxygen vacancy concentration.

The oxidation state of surface Ag was examined analyzing the Ag $3d_{5/2}$ peak in XPS spectra for both IM and SG catalysts (Fig. 5, 1A and 1B). The Ag $3d_{5/2}$ spectra were deconvoluted into three components and their positions are presented in Table 4. Three components named Ag^{I}, Ag^{II} and Ag^{III} were detected at 368.1, 368.7 and 369.7 eV. The assignment of Ag oxidation state by XPS is non-trivial because Ag is a metal that has anomalous properties in BE shifts when being oxidized, i.e. the Ag 3d peaks shift to lower BE values relative to metallic silver. The observed negative shifts of the Ag 3d XPS peak upon oxidation are linked to several factors including lattice potential, work function changes and extra-atomic relaxation energy [33]. Moreover, the same silver chemical states revealed differences in Ag $3d_{5/2}$ BE values within a 1.2 eV interval and even superimpositions, thus making the assignment of the observed peaks a rather difficult task [34]. Thus, only Ag^{III} with BE of 369.7 eV can be clearly assigned to the Ag nanoparticles at the surface of both catalysts [21]. The position of the Ag^{I} and Ag^{II} implies that they represent silver atoms in an oxidized and metallic state, respectively.

In order to further explore the electronic state of Ag in the studied catalysts, the AgMNN Auger peaks were also recorded (Fig. 5, 2A and 2B) and the modified Auger parameter was calculated (α = Ag $3d_{5/2}$ (BE) + $AgM_4N_{45}N_{45}$ (KE)) using the center of the recorded XPS and Auger peaks. As shown in Table 4, the values were in the range of 725.4-725.8 eV, slightly lower than the value of 726.1 eV that was reported [30] for metallic Ag but significantly higher than the values of 724.5 and 724.0 eV for Ag_2O and AgO, respectively. The difference in Auger parameters between the metallic Ag reported in the literature and those obtained from the IM and SG catalyst may indicate the presence of Ag cationic species on the catalyst surface. This difference was higher for the IM sample supposing the higher concentration of oxidized Ag, but further studies are needed for confirmation. Based on the above considerations, one can conclude that both catalysts contained surface metallic Ag atoms, which were represented by the Ag $3d_{5/2}$ component at around 368.5 eV (Ag^{II}) while the Ag^{I} component can be attributed to partially oxidized silver species.

Table 4 shows that the SG sample contained 60% metallic silver (Ag^{II}) compared to 47% in the IM sample. The Ag/Zr atomic ratios shown in Table 4 for both catalysts were much lower than the nominal bulk Ag/Zr ratio of ~0.43. This implies Ag deficiency on the surface for both catalysts regardless the preparation method. The SG method provided a greater surface enrichment in Ag compared to the IM method as shown by the higher Ag/Zr ratio of 0.18.

3.5. O_2-TPD

O_2-TPD was carried out for all SG and IM Ag/ZrO_2 catalysts with varying Ag loading to investigate the effect of the preparation method on oxygen activation. Fig. 6 depicts the O_2 desorption profiles for both series of catalysts and the corresponding supports. Firstly, the oxygen desorption from the IM and SG catalysts with 5 mol% Ag exhibited peaks at the same temperature of 350 °C. Secondly, the SG catalysts O_2-TPD desorption peaks positions and intensities changed significantly with the increase of Ag loading while all Ag/ZrO_2-IM catalysts demonstrated very similar TPD profiles regardless of the Ag loading

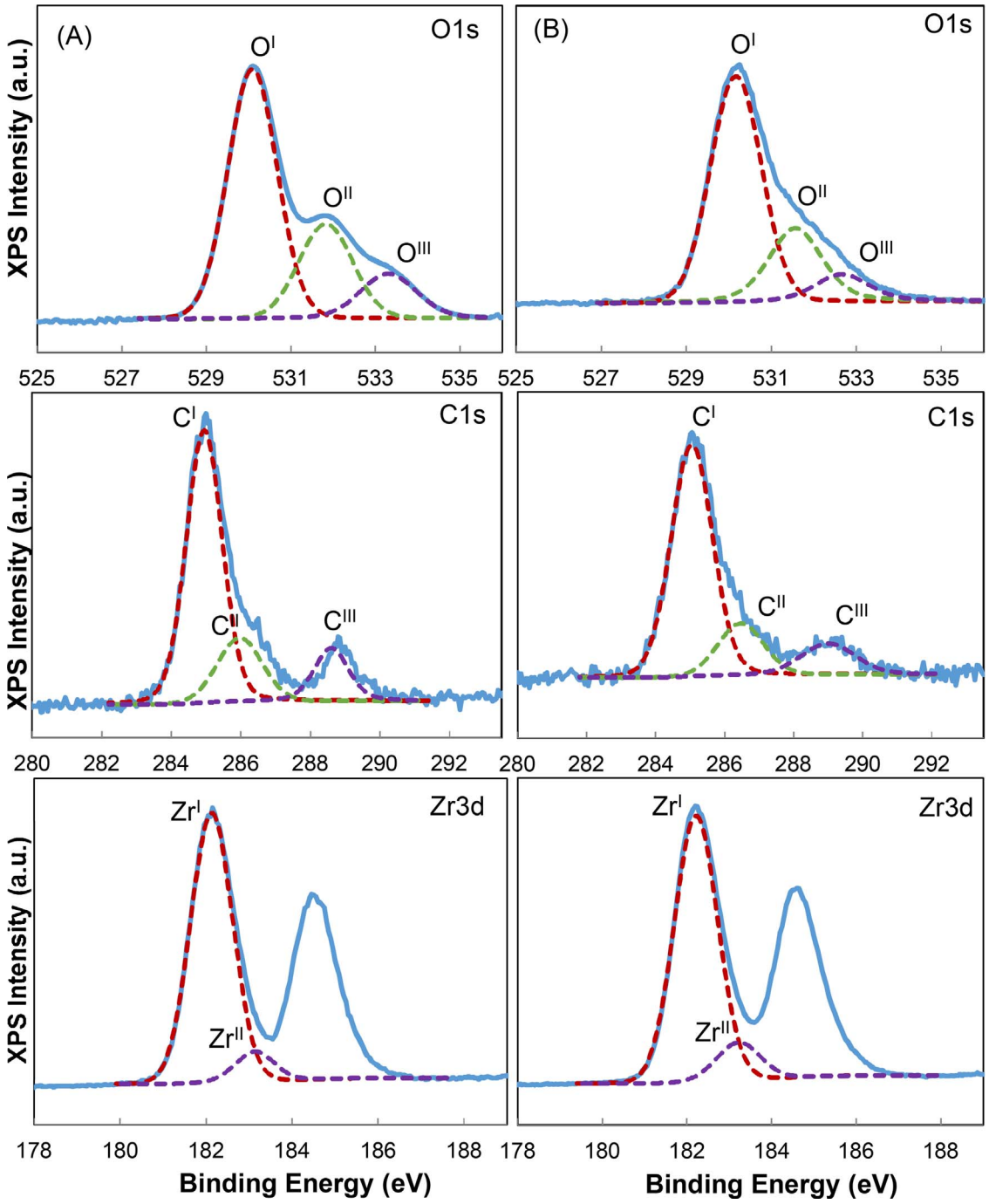

Fig. 4. O 1s, C 1s and Zr 3d XPS spectra for the Ag(30)/ZrO_2-IM (A) and Ag(30)/ZrO_2-SG (B) catalysts.

(Fig. 6). Thirdly, the asymmetric form of all the TPD peaks of both SG and IM catalysts suggested the existence of several types of oxygen species adsorbed on the Ag-zirconia catalysts. Additionally, O_2 desorption from the bare SG ZrO_2 was observed at temperatures above 300 °C whereas commercial ZrO_2 did not show any desorption up to 460 °C.

Deconvolution of the O_2-TPD profiles was performed using a straight line from 240 °C to 400 °C for the baseline subtraction to identify the desorption peaks of each type of oxygen. Fig. S4 shows the deconvolution results for both series of catalysts. Based on the calculations, we distinguished two types of oxygen species desorbed from the catalysts: O-I and O-II with temperature peaks at 270–300 °C and 310–350 °C, respectively. Additionally, it should be noted that desorption of O_2 continued at higher temperature up to 550 °C for both SG and IM catalysts. However, these oxygen species were not taken into consideration because soot oxidation on these catalysts occurred at lower temperatures between 200 and 400 °C.

There are numerous studies on oxygen interaction with supported and unsupported Ag catalysts. The low-temperature peaks in the O_2-TPD profiles were attributed to weakly chemisorbed atomic oxygen (150–350 °C), and the high-temperature desorption peaks were assigned to strongly chemisorbed atomic oxygen in the bulk and subsurface Ag layers (400–750 °C) [35–40]. Additionally, several distinct states may exist within each type of oxygen species. Atkins et al. [41] observed two low temperature oxygen desorption peaks at 250 °C and 300 °C from Ag/α-Al_2O_3 catalysts. Bal'zhinimaev's paper [42] distinguished two states of adsorbed atomic surface oxygen based on their Ag—O bonding differences. Bal'zhinimaev assigned the lower

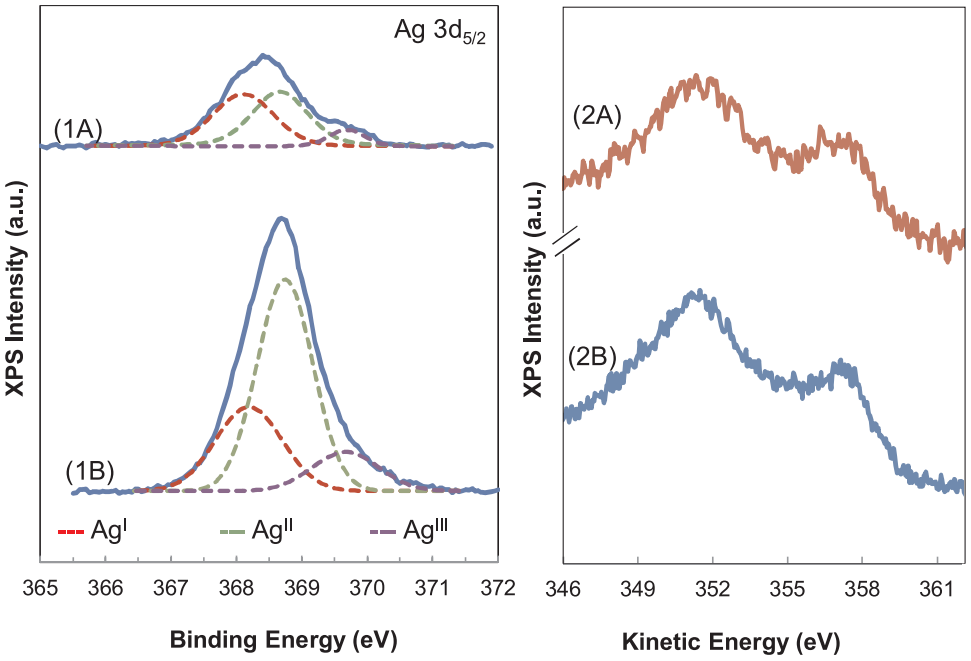

Fig. 5. Ag $3d_{5/2}$ XPS peaks deconvoluted with three components for the Ag(30)/ZrO_2-IM (1A) and Ag (30)/ZrO_2-SG (1B) catalysts and AgMNN X-AES peaks for the Ag(30)/ZrO_2-IM (2A) and Ag(30)/ZrO_2-SG (2B) catalysts.

temperature peak to nucleophilic oxygen atoms exhibiting Ag—O—Ag bonding on Ag regular surface (*e.g.* Ag terrace sites). The higher temperature peak was attributed to electrophilic oxygen possessing stronger Ag = O bonding when adsorbed on defect regions of the silver surface. According to the data obtained by Tsybulya et al. [43], there were two types of abundant defects in silver particles: grain boundaries/boundaries of twining and packing defects. Tsybulya et al. showed that the catalyst treatment in oxidative or reaction atmospheres annealed the packing defects easily, while intergrain boundaries were stable.

Based on the literature data reported above, we assigned our oxygen thermodesorption peaks: O-I to nucleophilic oxygen and O-II to electrophilic. According to the literature [42], nucleophilic oxygen formed on regular surface obtained by large particles (likely, micrometer-size). On the other hand, small particles (likely, nanometer-size) with higher concentration of defects favoured to the formation of electrophilic type of oxygen. The quantities of each oxygen species and the peak positions are reported in Table 5. When Ag concentration increased from 5 up to 30 mol%, the number of large particles responsible for the O-I formation also increased. However, higher concentration of regular surfaces accessible for adsorption was counterbalanced by decreasing the exposed Ag surface areas. Therefore, only a small shoulder of O-I appeared in the O_2-TPD profiles for the IM catalysts. On the other hand, O-I continuously increased with Ag content for SG catalysts. The process of Ag sintering seems to be less pronounced for SG catalysts. As a result, the size of Ag particles did not reach such a high value as for IM catalysts and Ag surface exposed to oxygen adsorption remained higher than that of IM catalysts with the same Ag content.

Comparison of the amounts of O-II species between SG and IM catalysts showed comparable values of O-II for both catalysts indicating probably similar number of defective small Ag particles.

The total amount of O_2 (O-I and O-II) is shown in Table 5. The results clearly demonstrated a significant increase in O_2 desorption for the SG catalysts with an increase in Ag loading whereas there were no significant changes in the amount of desorbed oxygen for the IM catalysts. It has been shown in some studies [6,11] that oxygen species adsorbed on the catalyst surface acted as active species for soot oxidation due to the clear correlation between O_2 desorption and catalytic activity. Related to this work, SG catalysts produced more active oxygen species for soot oxidation compared to the IM catalysts. The O_2-TPD data strongly supports the hypothesis that the preparation method does affect the chemical properties of silver-zirconia catalysts.

3.6. Catalytic activity tests

The silver-zirconia catalysts were initially tested using TPO runs carried out with 10 vol% O_2/He in order to validate the effects of the preparation method and Ag loading on catalyst efficiency for CB oxidation. The values of T_{max} from the TPO profiles of two series of Ag-zirconia catalysts prepared by either IM or SG methods as a function of

Table 4
XPS parameters of the O 1s, C 1s and Zr $3d_{5/2}$ and Ag $3d_{5/2}$ for the Ag(30)/ZrO_2-IM and Ag(30)/ZrO_2-SG catalysts.

Catalyst	O 1s[a]		C 1s[a]		Zr $3d_{5/2}$[a]		Ag $3d_{5/2}$[a]		Auger Parameter[b] (eV)	Atomic Ratios	
	BE (eV)	%[c]	BE (eV)	%[c]	BE (eV)	%[c]	BE (eV)	%[c]		O/Zr	Ag/Zr
Ag(30)/ZrO_2-IM	530.1(O^I)	62	285.0 (C^I)	67	182.1(Zr^I)	90	368.1(Ag^I)	45	725.4	2.5	0.12
	531.7(O^{II})	25	286.5(C^{II})	19	183.2(Zr^{II})	10	368.7(Ag^{II})	47			
	533.2(O^{III})	13	289.0 (C^{III})	14			369.7(Ag^{III})	8			
Ag(30)/ZrO_2-SG	530.2(O^I)	66	285.0 (C^I)	70	182.2(Zr^I)	88	368.2(Ag^I)	29	725.8	2.3	0.18
	531.6(O^{II})	25	286.5(C^{II})	17	183.2(Zr^{II})	12	368.8(Ag^{II})	60			
	532.9(O^{III})	9	289.0 (C^{III})	13			369.7(Ag^{III})	11			

[a] obtained by deconvolution of XPS peaks.
[b] obtained using the center of peaks.
[c] fraction of each peak over the total sum of all peaks obtained by deconvolution.

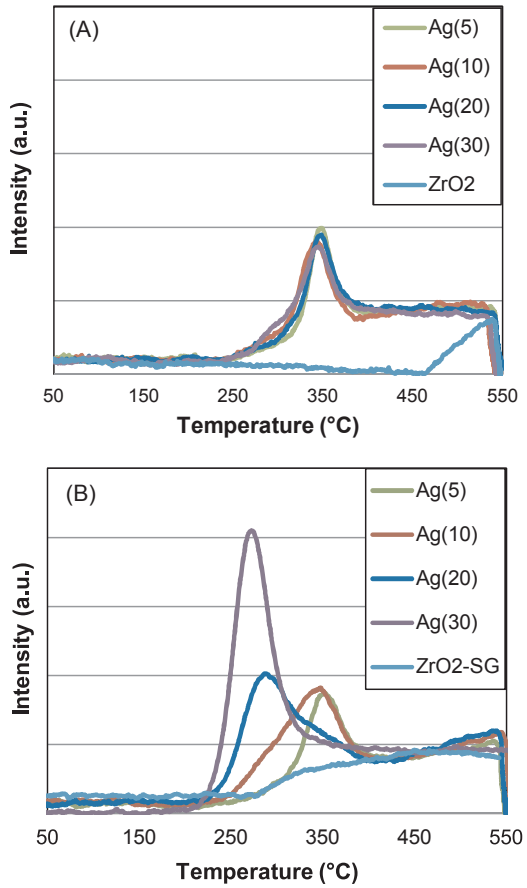

Fig. 6. O_2-TPD profiles of Ag/ZrO_2 catalysts with different Ag loading: A − IM catalysts, B − SG catalysts.

Table 5
O_2 desorption from O_2-TPD obtained for Ag/ZrO_2 catalysts.

Catalyst	O_2-TPD parameters				O_2 desorption[b] (μmol/g_{cat})
	Peak T[a] (°C)		Peak Area (O_2 μmol/g_{cat})		
	O-I	O-II	O-I	O-II	
$Ag(5)/ZrO_2$-IM	n.d.[c]	347	n.d.	0.93	0.93
$Ag(10)/ZrO_2$-IM	289	340	0.09	1.05	1.14
$Ag(20)/ZrO_2$-IM	n.d.	347	n.d.	0.92	0.92
$Ag(30)/ZrO_2$-IM	300	343	0.17	0.91	1.08
$Ag(5)/ZrO_2$-SG	n.d.	351	n.d.	1.01	1.01
$Ag(10)/ZrO_2$-SG	301	345	0.60	1.20	1.80
$Ag(20)/ZrO_2$-SG	284	332	1.58	1.00	2.58
$Ag(30)/ZrO_2$-SG	271	307	3.13	1.34	4.47

[a] Peak temperature in O_2-TPD profiles.
[b] amount of O_2 desorption calculated in temperature range from 240 to 400 °C.
[c] not determined.

silver loading are shown in Table 6. Analysis of the relationship between T_{max} and the Ag loading revealed a significant difference between catalysts prepared by the IM and SG preparation methods. Increasing the silver content from 5 to 10 mol% led to a slight decrease of

Table 6
CB oxidation performance data of Ag/ZrO_2 catalysts in TPO runs.

Catalyst	T_{max}[a] (°C)	Specific Activity[b]	Catalyst	T_{max}[a] (°C)	Specific Activity[b]
$Ag(5)/ZrO_2$-IM	402	1.57	$Ag(5)/ZrO_2$-SG	398	2.00
$Ag(10)/ZrO_2$-IM	398	1.25	$Ag(10)/ZrO_2$-SG	385	1.82
$Ag(20)/ZrO_2$-IM	404	1.21	$Ag(20)/ZrO_2$-SG	377	3.08
$Ag(30)/ZrO_2$-IM	405	1.32	$Ag(30)/ZrO_2$-SG	371	5.21

[a] T_{max} in TPO profiles.
[b] the rate of catalytic reaction at 350 °C normalized to the Ag surface area in mmol/m^2 Ag/sec.

T_{max} for IM catalysts. However, further increase of silver up to 30 mol% did not improve the catalytic activity of the IM catalysts as demonstrated by the T_{max} near 405 °C for both $Ag(20)/ZrO_2$-IM and $Ag(30)/ZrO_2$-IM. Among the IM catalysts, the best performing catalysts contained 5 and 10 mol% Ag exhibiting almost identical values of T_{max} of 400 and 398 °C, respectively.

On the other hand, Ag/ZrO_2-SG catalysts showed a significant decrease of 27 °C in T_{max} as their Ag content increased from 5 to 30 mol%. The most active SG catalyst containing 30 mol% Ag exhibited a T_{max} of 371 °C which was much lower than those for CB oxidation over a commercial zirconia (613 °C) and non-catalytic CB oxidation (678 °C).

Additionally, the rates of CB oxidation were measured under isothermal conditions at 350 °C using a TGA instrument (Fig. S5). Table 6 shows the values of specific catalytic activity which were calculated by normalizing the reaction rates to the Ag surface area obtained by O_2-chemisortption experiments. As one can see, the catalytic activity per unit of accessible Ag surface area was approximately constant for IM catalysts regardless of Ag content. On the contrary, SG catalysts exhibited an increase of specific activity when the Ag concentration varied from 5 to 30 mol%. Thus, the differences in catalytic performance between the two series of catalysts was not simply due to the difference in Ag surface area of the IM and SG catalysts. Characterization results showed that silver-zirconia catalysts differed significantly in their surface morphology and structural characteristics which in turn influenced their oxygen adsorption and catalytic properties.

Overall, Ag/ZrO_2-SG catalysts performed better than those prepared by impregnation, irrespective of Ag content.

The best performing $Ag(30)/ZrO_2$-SG catalyst was selected for further evaluation using a fixed-bed reactor with simulated diesel exhaust gas compositions. Fig. 7 displays the carbon dioxide concentration versus temperature profiles for runs using different feed gas composition. Testing with 10 vol% O_2 in nitrogen determined that the T_{max} in the experimental profile was 338 °C (Fig. 7, red curve). This test clearly confirmed the ability of silver-zirconia catalyst to convert CB completely to CO_2 using oxygen in the temperature range from 200 °C to 400 °C, typical of diesel exhaust. The next evaluation was carried out under a gas flow containing 10 vol% O_2, 5 vol% water vapour in nitrogen. The data (Fig. 7, blue curve) revealed a significant increase in activity resulting in a T_{max} of 290 °C, which is 50 °C lower than without water in the feed gas. A possible reason for the positive effect of water was shown to be the stabilization of surface oxygen species which are responsible for the carbon oxidation by O_2 [44]. In addition, these authors suggested that water can catalytically promote the oxidation of CO produced through carbon gasification and/or carbon oxidation, thus leading to enhancement of the overall combustion rate. Further investigation of the water effect on catalytic soot oxidation is needed before the reaction mechanism of soot oxidation in presence of water can be confirmed.

The CB oxidation on the $Ag(30)/ZrO_2$-SG catalyst was also tested

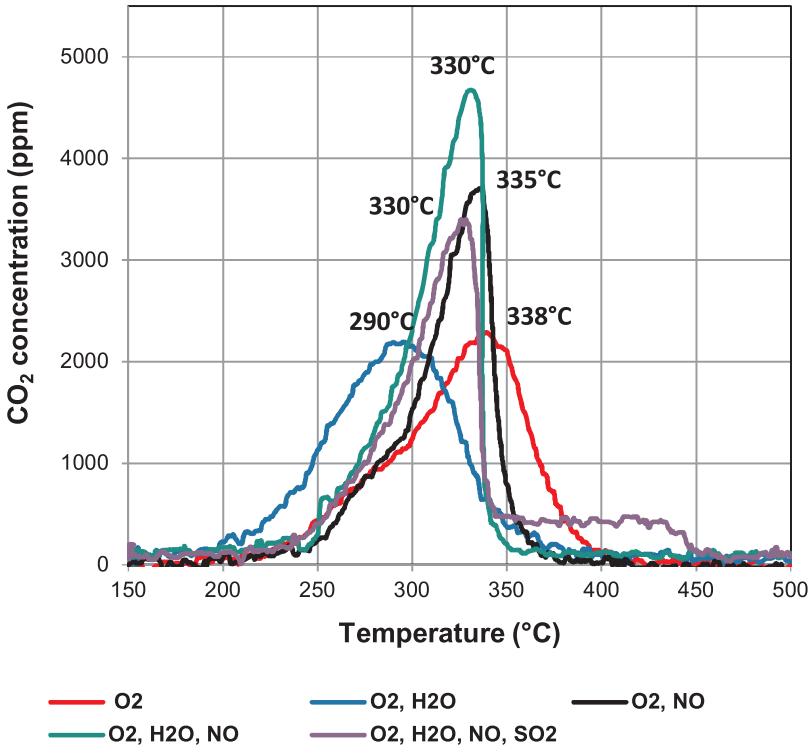

Fig. 7. Effect of reaction gas composition on the activity of Ag(30)/ZrO_2-SG catalyst during simulated diesel exhaust gas test. Feed gas component concentrations: 10 vol% O_2, 5 vol% H_2O, 500 ppm NO, 10 ppm SO_2 in nitrogen.

with nitric oxide (500 ppm NO) being added to the feed gas containing 10 vol% O_2 (Fig. 7, black curve). The obtained T_{max} value of 335 °C was slightly lower than that for the same experiment carried out without NO. Testing with 10 vol% O_2, 5% vol% H_2O, 500 ppm NO in a feed gas (Fig. 7, green curve) showed a T_{max} of 330 °C which was higher by 40 °C than that obtained in the run with O_2 and water. Thus, NO did not appear to accelerate the soot oxidation rate significantly in contrast to platinum-based catalysts which were shown to accelerate soot oxidation in the presence of NO in a feed gas [3]. In our study, it seemed that the CB oxidation with O_2 alone on silver-zirconia catalyst under tight contact took place so effectively that the presence of NO did not significantly benefit the reaction. Therefore, the most pronounced effect of NO could be apparent under loose contact testing conditions. The same observation was reported by Matarrese et al. [45] who showed little effect of NO_x on soot combustion on Pt-K/Al_2O_3 and Pt-Ba/Al_2O_3 catalysts under tight contact conditions whereas a shift in T_{max} towards low temperature of 50–100 °C was observed for the same catalysts under loose contact with carbon. Zouaoui et al. [46] also reported that the activation energy of soot oxidation with oxygen on CeO_2 catalyst was lower than that with O_2 + NO mixture (44 versus 59 kJ/mol) under tight conditions. Loose contact conditions revealed an opposite trend in the activation energy for soot oxidation depending on the reaction gas composition (135 and 72 kJ/mol in O_2 and O_2 + NO, respectively).

The resistance to sulfur poisoning of Ag(30)/ZrO_2-SG was also tested using a flow containing 500 ppm NO, 10 vol% O_2, 5 vol% H_2O with the addition 10 ppm of SO_2 (Fig. 7, purple curve). The observed T_{max} of 330 °C in this test demonstrated the same CB activity as that under the previous gas composition without sulfur oxide. This observation clearly demonstrated high sulfur tolerance of the catalyst. The sulfur resistance of silver-zirconia catalysts may be due to the zirconia acting as a trap for the sulfates. It has been shown that formation of surface sulfates on zirconia occurred after being exposed to SO_2 with an excess of oxygen [47]. It appears that zirconia assisted in the removal of sulfur oxides from the feed. Therefore, zirconia prevents poisoning of Ag active sites that are responsible for oxygen activation required for the reaction. Furthermore, an unusual promotion effect of SO_2 on the carbon oxidation over Pt/SiO_2 catalyst under loose contact conditions was reported [48] when SO_2 was added to a feed mixture of NO, O_2 and H_2O. Those authors speculated that SO_3 (or H_2SO_4) formed from SO_2 over Pt could catalyze carbon oxidation by NO_2. However, in the present study, no improvement of the CB oxidation activity by SO_2 addition was observed, probably due to the tight contact conditions that were used.

Finally, Ag(30)/ZrO_2-IM and the Ag(30)/ZrO_2-SG catalysts were evaluated for soot oxidation performance under diesel simulated conditions after they were loaded with soot using a soot generator. This type of soot loading represented similar contact between soot and catalyst particles encountered in a real industrial application. The soot conversion as a function of temperature of the IM and SG soot loaded catalysts are shown in Fig. 8. It is evident that the soot conversion obtained for the SG catalyst was higher than that for the IM catalyst over the whole temperature region from 200 to 500 °C. The T_{50} value

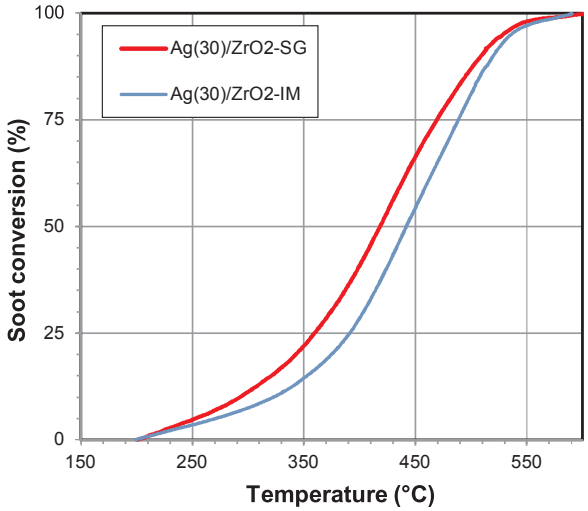

Fig. 8. CO_2 concentration as a function of temperature during oxidation of soot loaded on Ag(30)/ZrO_2-SG and Ag(30)/ZrO_2-IM catalysts from soot generator. Feed gas component concentrations: 10 vol% O_2, 5 vol% H_2O, 500 ppm NO in nitrogen.

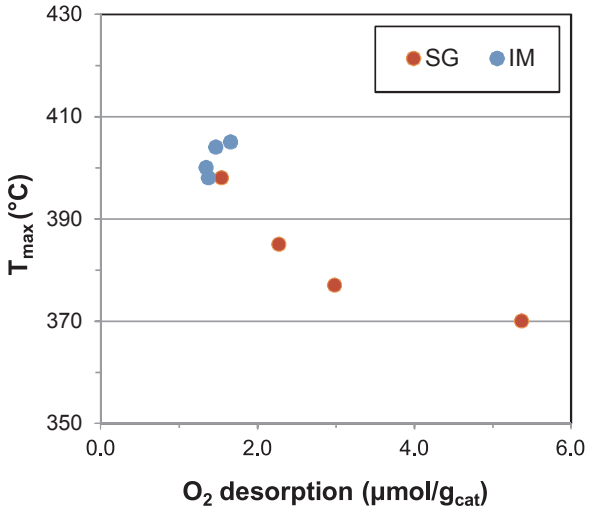

Fig. 9. T_{max} values from TPO experiments as a function of desorbed oxygen amount from O_2-TPD for the IM and SG Ag/ZrO_2 catalysts.

that corresponded to 50% of soot conversion was 418 °C for the SG catalyst that was lower by 25° than that of the IM catalyst. This preliminary test under more realistic soot loading conditions strongly suggests that the Ag(30)/ZrO_2-SG catalyst is a suitable candidate for future study using a diesel engine.

3.7. Structure-property relationship

O_2-TPD experiments showed that IM and SG catalysts performed very differently when adsorbing O_2 from the gas phase. Fig. 9 shows the dependencies of the CB oxidation activity and the amount of O_2 desorbed in the temperature range between 200 °C to 450 °C where the catalysts were active. One can see that data are in an excellent agreement. These results strongly support the assumption that surface oxygen species on the Ag surface played an important role in the carbon oxidation when carbon particles are in close proximity to Ag particles. It can be speculated that there are some predominant steps in the CB oxidation mechanism on both SG and IM Ag/ZrO_2 catalysts. Firstly, silver particles create the shell of active oxygen species on their surface through adsorption of oxygen from the gas phase. Then, carbon is oxidized at the carbon-silver interfaces involving adjacent active oxygen atoms. Oxygen species consumed during reaction are continuously restored by oxygen dissociative adsorption from the gas phase or by a migration of oxygen species along the Ag surface to the contact area. Another source for refilling consumed surface oxygen species is oxygen diffusion from Ag subsurface to the external surface of Ag particles. Additionally, the bare zirconia exhibited its ability to adsorb oxygen from the gas phase (Fig. 7), therefore interface of Ag and ZrO_2 can act as the active phase for the CB oxidation. Despite that, these steps are common for both series of catalysts, the observed difference in catalytic performance of IM and SG catalysts indicates that the preparation method influences all suggested reaction pathways.

Firstly, the citrate sol-gel method yields silver-zirconia catalysts where Ag particles undergo lower sintering compared to IM catalysts according to the SEM images (Fig. 3). Smaller micrometer-size Ag particle for the SG catalyst created higher surface area for oxygen adsorption (O-I, nucleophilic oxygen) from the gas phase resulting in higher activity. The stability of Ag particles on the SG zirconia can be related to the oxygen vacancies according to researchers [49]. They found that the formation of oxygen vacancies in CeO_2 led to the self-dispersion of Ag particles. In our study, the SG zirconia desorbed oxygen in larger amounts and at lower temperature compared to the commercial monoclinic zirconia as shown in Fig. 6. We assume that this difference is due to the higher concentration of oxygen vacancies formed in the SG tetragonal zirconia compared to the monoclinic zirconia used for IM catalysts. As a result, oxygen vacancies in the non-stoichiometric tetragonal zirconia assisted in stabilization of Ag particles in SG catalysts.

Secondly, oxygen vacancies in the tetragonal zirconia itself participated in oxygen adsorption and surface-capping oxygen of zirconia could refill the external surface of Ag. The SG preparation method produced silver-zirconia catalysts with decreased crystal sizes of zirconia in the range of 7.3–12.6 nm compared to the 20 nm crystal size of the monoclinic zirconia for the IM catalysts. This led to the formation of higher concentration of oxygen vacancies and sequentially higher number of surface oxygen enabling to take part in the reaction. It should be mentioned also that the crystal size of zirconia decreased and a fraction of tetragonal zirconia in the SG catalyst increased with the Ag loading. This finding suggests that Ag interacts with the support and helps to stabilize tetragonal phase of zirconia.

Thus, it can be concluded that the citrate sol-gel preparation method induced a strong synergy between silver and zirconia that resulted in higher oxygen adsorption and higher carbon oxidation activity compared to conventional catalyst impregnation.

4. Conclusions

This study demonstrated that the catalyst preparation method significantly influences the physical and catalytic properties of silver-zirconia catalysts. The best performing silver-zirconia catalyst for CB oxidation was determined to be the Ag(30)/ZrO_2-SG catalyst. The differences in activity between incipient wetness impregnation and sol-gel catalysts were explained by microstructural, morphological and phase composition differences. The amounts of desorbed oxygen correlated very well with the values of T_{max} obtained in TPO runs indicating that adsorbed atomic oxygen played a major role in the mechanism of CB oxidation. The citrate sol-gel preparation method was shown to induce higher synergy between silver and zirconia support in CB oxidation.

In conclusion, the Ag(30)/ZrO_2-SG catalyst was experimentally shown to be a promising candidate for application in a catalyzed DPF for oxidizing soot with O_2 in the temperature range of diesel exhaust (O_2-based technology). It could be used as an alternative to NO_2-based technology, which uses expensive Pt catalyst. The results obtained in this study provide valuable information to be used for the design of advanced catalytic systems for soot removal from diesel engine exhaust.

Acknowledgements

Funding for this project was provided by Natural Resources Canada through the Program on Energy Research and Development (PERD) – Advanced Fuels and Technologies for Emissions Reduction (AFTER). The authors would also like to thank Dr. N. Maffei for fruitful discussions, Mr. Raymond Burich for catalyst testing and Mr. Nikolay Videnov for O_2-TPD deconvolution calculations.

Appendix A. Supplementary data

Supplementary data associated with this article can be found, in the online version, at https://doi.org/10.1016/j.apcatb.2017.11.070.

References

[1] US Environmental Protection Agency: Report to Congress on Black Carbon, http://www.epa.gov/blackcarbon/2012report/fullreport.pdf (accessed July, 2017).
[2] B.J. Cooper, H.J., Jung, J.E. Thoss, Treatment of diesel exhaust gases, US Patent 4902487, 1990.
[3] Johnson Matthey: The Continuously Regenerating Trap. http://www.matthey.com/innovation/history/continuously_regenerating_trap (accessed July, 2017).
[4] US Drive Report: Future Automotive Aftertreatment Solutions: The 150 °C Challenge Workshop Report, (2012) http://www.pnnl.gov/main/publications/external/technical_Reports/PNNL-22815.pdf (accessed July, 2017).
[5] E. Aneggi, J. Llorca, C. de Leitenburg, G. Dolcetti, A. Trovarelli, Soot combustion

over silver-supported catalysts, Appl. Catal. B Environ. 91 (2009) 489–498, http://dx.doi.org/10.1016/j.apcatb.2009.06.019.
[6] K. Yamazaki, T. Kayama, F. Dong, H. Shinjoh, A mechanistic study on soot oxidation over CeO_2-Ag catalyst with rice-ball morphology, J. Catal. 282 (2011) 289–298, http://dx.doi.org/10.1016/j.jcat.2011.07.001.
[7] M. Machida, Y. Murata, K. Kishikawa, D. Zhang, K. Ikeue, On the reasons for high activity of CeO_2 catalyst for soot oxidation, Chem. Mater. 20 (2008) 4489–4494, http://dx.doi.org/10.1021/cm800832w.
[8] N. Guilhaume, B. Bassou, G. Bergeret, D. Bianchi, F. Bosselet, A. Desmartin-Chomel, B. Jouguet, C. Mirodatos, In situ investigation of diesel soot combustion over an $AgMnO_x$ catalyst, Appl. Catal. B Environ. 119-120 (2012) 287–296, http://dx.doi.org/10.1016/j.apcatb.2012.03.009.
[9] G. Corro, U. Pal, E. Ayala, E. Vidal, Diesel soot oxidation over silver-loaded SiO_2 catalysts, Catal. Today. 212 (2013) 63–69, http://dx.doi.org/10.1016/j.cattod.2012.10.005.
[10] C. Lee, J.-I. Park, Y.-G. Shul, H. Einaga, Y. Teraoka, Ag supported on electrospun macro-structure CeO_2 fibrous mats for diesel soot oxidation, Appl. Catal. B Environ. 174–175 (2015) 185–192, http://dx.doi.org/10.1016/j.apcatb.2015.03.008.
[11] T. Nanba, S. Masukawa, A. Abe, J. Uchisawa, A. Obuchi, Morphology of active species of Ag/ZrO_2 for low-temperature soot oxidation by oxygen, Catal. Sci. Technol. 2 (2012) 1961–1966, http://dx.doi.org/10.1039/c2cy00546h.
[12] M. Haneda, A. Towata, Catalytic performance of supported Ag nano-particles prepared by liquid phase chemical reduction for soot oxidation, Catal. Today 242 (2015) 351–356, http://dx.doi.org/10.1016/j.cattod.2014.05.044.
[13] G. Pecchi, R. Dinamarca, C.M. Campos, X. Garcia, R. Jimenez, J.L.G. Fierro, Soot oxidation on silver-Substituted $LaMn_{0.9}Co_{0.1}O_3$ perovskites, Ind. Eng. Chem. Res. 53 (2014) 10090–10096, http://dx.doi.org/10.1021/ie501277x.
[14] K. Shimizu, H. Kawachi, A. Satsuma, Study of active sites and mechanism for soot oxidation by silver-loaded ceria catalyst, Appl. Catal. B, Environ. 96 (2010) 169–175, http://dx.doi.org/10.1016/j.apcatb.2010.02.016.
[15] M.P. Pechini, N. Adams, Method of preparing lead and alkaline earth titanates and niobates and coating method using the same to form a capacitor, US Patent 3330697, (1967).
[16] J.A. Schwarz, C. Contescu, A. Contescu, Methods for preparation of catalytic materials, Chem. Rev. 95 (1995) 477–510.
[17] S.R. Seyedmonir, D.E. Strohmayer, G.L. Geoffroy, M.A. Vannice, Characterization of supported silver catalysts 1. adsorption of O_2, H_2 N_2O, and H_2-titration of adsorbed oxygen on well-dispersed Ag on TiO_2, J. Catal. 87 (1984) 424–436.
[18] K.S.W. Sing, D.H. Everett, R.W. a. Haul, L. Moscou, R. a. Pierotti, J. Rouquérol, T. Siemieniewska, Reporting physisorption data for gas/solid systems with special reference to the determination of surface area and porosity, Pure Appl. Chem. 57 (1985) 603–619, http://dx.doi.org/10.1351/pac198557040603.
[19] F. Namavar, G. Wang, C.L. Cheung, R.F. Sabirianov, X.C. Zeng, W.N. Mei, J. Bai, J.R. Brewer, H. Haider, K.L. Garvin, Thermal stability of nanostructurally stabilized zirconium oxide, Nanotechnology 18 (2007) 415702–415708, http://dx.doi.org/10.1088/0957-4484/18/41/415702.
[20] R. Malakooti, H. Mahmoudi, R. Hosseinabadi, S. Petrov, A. Migliori, Facile synthesis of pure non-monoclinic zirconia nanoparticles and their catalytic activity investigations for Knoevenagel condensation, RSC Adv. 3 (2013) 22353–22359, http://dx.doi.org/10.1039/c3ra44682d.
[21] R. Grabowski, J. Sloczynski, M. Sliva, D. Mucha, R.P. Socha, M. Lachowska, J. Skrzypek, Influence of polymorphic ZrO_2 phases and the silver electronic state on the activity of Ag/ZrO_2 catalysts in the hydrogenation of CO_2 to methanol, ACS Catal. 1 (2011) 266–278, http://dx.doi.org/10.1021/cs100033v.
[22] S. Fabris, A.T. Paxton, M.W. Finnis, A stabilization mechanism of zirconia based on oxygen vacancies only, Acta Mater. 50 (2002) 5171–5178.
[23] R.C. Garvie, The occurrence of metastable tetragonal zirconia as a crystallite size effect, J. Phys. Chem. 69 (1965) 1238–1243, http://dx.doi.org/10.1021/j100888a024.
[24] O.Y. Kurapova, V.G. Konakov, Phase evolution in zirconia based systems, Rev. Adv. Mater. Sci. 36 (2014) 177–190.
[25] S.N. Basahel, T.T. Ali, M. Moukhtar, K. Narasimharao, Influence of crystal structure of nanosized ZrO_2 on photocatalytic degradation of methyl orange, Nanoscale Res. Lett. 73 (2015) 1–13, http://dx.doi.org/10.1186/s11671-015-0780-z.
[26] J.A. Navio, C. Hidalgo, G. Colon, S.G. Botta, M.I. Litter, Photocatalytic properties of ZrO_2 and Fe/ZrO_2 semiconductors prepared by a sol – gel technique, Langmuir 17 (2001) 202–210.
[27] T.C.R. Rocha, A. Oestereich, D.V. Demidov, S. Zafeiratos, G. Weinberg, V.I. Bukhtiyarov, The silver – oxygen system in catalysis: new insights by near ambient pressure X-ray photoelectron spectroscopy w, Phys.Chem.Chem.Phys 14 (2012) 4554–4564, http://dx.doi.org/10.1039/c2cp22472k.
[28] V.I. Bukhtiyarov, M. Hävecker, V.V. Kaichev, R.W. Mayer, R. Schlögl, The nature of atomic oxygen species on silver: photoelectron spectroscopy and X-ray absorption studies, Phys. Rev. 67 (2003) 1–12.
[29] S.A. Steiner, T.F. Baumann, B.C. Bayer, R. Blume, M.A. Worsley, W.J. MoberlyChan, E.L. Shaw, R. Schlögl, A.J. Hart, S. Hofmann, B.L. Wardle, Nanoscale zirconia as a nonmetallic catalyst for graphitization of carbon and growth of single- and multi-wall carbon nanotubes, J. Am. Chem. Soc. 131 (2009) 12144–12154, http://dx.doi.org/10.1021/ja902913r.
[30] M.P. Briggs, D. Seah, Practical surface analysis, Auger and X-ray photoelectron spectroscopy, first ed., Wiley, Chichester, New York, 1983.
[31] H. Xu, S. Yuan, Z. Wang, Y. Zhao, J. Fang, L. Shi, Graphene anchored with ZrO_2 nanoparticles as anodes of lithium ion betteries with enhanced electrochemical performance, RCS Adv. 4 (2014) 8472–8480, http://dx.doi.org/10.1039/c3ra47653g.
[32] H. Li, J. Ren, X. Qin, Z. Qin, J. Lin, Z. Li, Ni/SBA-15 catalysts for CO methanation: effects of V, Ce and Zr promoters, RSC Adv. 5 (2015) 96504–96517, http://dx.doi.org/10.1039/C5RA15990C.
[33] B. Xin, L. Jing, Z. Ren, B. Wang, H. Fu, Effects of simultaneously doped and deposited Ag on the photocatalytic activity and surface states of TiO_2, J. Phys. Chem. B. 109 (2005) 2805–2809, http://dx.doi.org/10.1021/jp0469618.
[34] A.M. Ferraria, A. Carapeto, A.M. Botelho do Rego, X-ray photoelectron spectroscopy: silver salts revisited X-ray photoelectron spectroscopy: silver salts revisited, Vacuum 86 (2012) 1988–1991, http://dx.doi.org/10.1016/j.vacuum.2012.05.031.
[35] D. Kondarides, Oxygen adsorption on supported silver catalysts investigated by microgravimetric and transient techniques, J. Catal. 143 (1993) 481–491, http://dx.doi.org/10.1006/jcat.1993.1291.
[36] G.W. Busser, O. Hinrichsen, M. Muhler, The temperature-programmed desorption of oxygen from an alumina-supported silver catalyst, Catal. Letters 79 (2002) 49–54, http://dx.doi.org/10.1023/A:1015300520227.
[37] C.T. Campbell, Atomic and molecular oxygen adsorption on Ag(111), Surf. Sci. 157 (1985) 43–60, http://dx.doi.org/10.1016/0039-6028(85)90634-X.
[38] G.I.N. Waterhouse, G. a. Bowmaker, J.B. Metson, Oxygen chemisorption on an electrolytic silver catalyst: a combined TPD and Raman spectroscopic study, Appl. Surf. Sci. 214 (2003) 36–51, http://dx.doi.org/10.1016/S0169-4332(03)00350-7.
[39] A. Nagy, G. Mestl, High temperature partial oxidation reactions over silver catalysts, Appl. Catal. A Gen. 188 (1999) 337–353, http://dx.doi.org/10.1016/S0926-860X(99)00246-X.
[40] Z. Qu, M. Cheng, W. Huang, X. Bao, Formation of subsurface oxygen species and its high activity toward CO oxidation over silver catalysts, J. Catal. 229 (2005) 446–458, http://dx.doi.org/10.1016/j.jcat.2004.11.043.
[41] M. Atkins, J. Couves, M. Hague, B.H. Sakakini, K.C. Waugh, On the role of Cs, Cl and subsurface O in promoting selectivity in $Ag/\alpha - Al_2O_3$ catalysed oxidation of ethene to ethene epoxide, J. Catal. 235 (2005) 103–113, http://dx.doi.org/10.1016/j.jcat.2005.07.019.
[42] V.I. Bal'zhinimaev, Ethylene epoxidation over silver catalysts, Kinet. Catal. 40 (1999) 795–810.
[43] S.V. Tsybulya, Study of the real structure of silver supported catalysts of different dispersity, J. Catal. 154 (1995) 194–200, http://dx.doi.org/10.1006/jcat.1995.1160.
[44] K. Matsui, H. Tsuji, A. Makino, A further study of the effects of water vapor concentration on the rate of combustion of an artificial graphite in humid air flow, Combust. Flame. 63 (1986) 415–427, http://dx.doi.org/10.1016/0010-2180(86)90008-8.
[45] R. Matarrese, L. Castoldi, L. Lietti, P. Forzatti, Soot combustion: reactivity of alkaline and alkaline earth metal oxides in full contact with soot, Catal. Today 136 (2008) 11–17, http://dx.doi.org/10.1016/j.cattod.2008.03.022.
[46] N. Zouaoui, M. Issa, D. Kehrli, M. Jeguirim, CeO_2 catalytic activity for soot oxidation under NO/O_2 in loose and tight contact, Catal. Today 189 (2012) 65–69, http://dx.doi.org/10.1016/j.cattod.2012.02.066.
[47] T. Luo, R. Gorte, Characterization of SO_2-poisoned ceria-zirconia mixed oxides, Appl. Catal. B Environ. 53 (2004) 77–85, http://dx.doi.org/10.1016/j.apcatb.2004.04.020.
[48] J. Oi-uchisawa, A. Obuchi, A. Ogata, R. Enomoto, S. Kushiyama, Effect of feed gas composition on the rate of carbon oxidation with Pt/SiO_2 and the oxidation mechanism, Appl. Catal. B, Environ. 21 (1999) 2–8.
[49] K. Shimizu, H. Kawachi, S. Komai, K. Yoshida, Y. Sasaki, A. Satsuma, Carbon oxidation with Ag/ceria prepared by self-dispersion of Ag powder into nano-particles, Catal. Today 175 (2011) 93–99, http://dx.doi.org/10.1016/j.cattod.2011.03.053.